Int. J. Electrochem. Sci., 13 **(2018)** 2509 – 2518, doi: 10.20964/2018.03.24

International Journal of
ELECTROCHEMICAL
SCIENCE
www.electrochemsci.org

Short Communication

Microstructures and Electrochemical Studies of Flux-Cored Arc and Flux-Copper Back Welded EH36 Steel

Kai Wang[1,2,*], *Qinghua Lu*[1], *Yaoyong Yi*[2], *Ben Niu*[2], *Jianglong Yi*[2], *Zexin Jiang*[3], *Jinjun Ma*[3]

[1]Foshan University, Foshan, Guangdong, 528000, China
[2]Guangdong Welding Institute (China-Ukraine E. O. Paton Institute of Welding), Guangzhou, Guangdong, 510651, China
[3]Guangzhou Shipyard International Co., Ltd, Guangzhou Guangdong, 510380, China
[*]E-mail: wk927@qq.com

Received: 19 February 2017 / *Accepted:* 25 December 2017 / *Published:* 5 February 2018

EH36 high strength steel plates were welded using flux-cored arc welding (FCAW) and flux copper backing (FCB) one-side submerged-arc welding (SAW) technology. The microstructure, microhardness distribution, and electrochemical behavior of the joints were studied. Because of the interaction of the thermal circle effect by the multi-layer and multi-pass welding modes of the FCAW, an asymmetric microhardness distribution resulted along the horizontal cross section lines caused by the softening phenomena. The high welding heat input FCB welding technology resulted in welding the joints with uniform microstructure and a symmetrical microhardness distribution along the horizontal cross section lines as well as a relatively stronger electrochemical behavior.

Keywords: High strength steel; FCAW; FCB; Microstructure; Electrochemical Impedance behavior

1. INTRODUCTION

The thermal mechanical control process (TMCP) combining a controlled rolling with an on-line accelerated cooling is now widely used to produce high strength steel plates. After hot rolling, the steel plates are immediately and rapidly cooled from a temperature of 800 °C to 500 °C using water and then air-cooled to room temperature. The microstructures of the TMCP steels are highly refined to significantly improve the strength and toughness of the steel, as reported by Wang et al. [1] and Xie et al. [2]. Thus TMCP EH36 steel is widely used in off-shore engineering and in the ship building industry.

Off-shore structures and ships have high requirements for the mechanical quality of welding joints. Lee et al. [3], Roepke C. et al. [4], and Tsay et al. [5] systematically studied the mechanical

properties of the welding joints of TMCP EH36 steel, showed that the welding joints are the weak points, and developed special welding materials and a method for high-efficiency welding of TMCP EH36 steel. Corrosion is always an important and unavoidable problem in off-shore engineering and in the ship building industry. In particular, corrosion of the welding joints in the ocean is more complicated, unavoidable, and severe. Ships and off-shore equipment are difficult to maintain and serve in a very corrosive and severe environment. As such, there are an abundance of problems caused by corrosion. However, little research has focused on the relationship between the microstructure, mechanical properties, and electrochemical properties of EH36 welding joints even though the welding joints serve for an extremely long time under seawater. By using the same welding consumables and base metals (BM), the properties of the welding joints mainly depend on the characteristics of the welding technology. Variation in electrochemical behavior can be controlled by maintaining the welding parameters in a certain range to obtain welding joints with excellent properties, as studied by Bhagavathi et al. [6]. Hu et al. [7] suggested that the welding heat input is an aggregative indicator of welding technology conditions such as welding current, voltages, and speeds, and is a key factor for deciding the combination of properties of the welding joints.

Flux-cored arc welding (FCAW) is a semi-automatic or automatic arc welding process that has been widely studied, such as in the work reported by Zhang et al. [8] and Chen et al. [9]. FCAW involves fusion of a flux-cored wire metal and/or a base metal with a welding heat input that is usually below 30~40 kJ/cm. Yan et al. [10] experimented with the flux copper backing (FCB) one-side submerged arc welding (SAW) technology, using three electrodes to understand single-face welding with double-face forming, to greatly improve the welding efficiency via a high welding heat input over 150 kJ/cm. However, comparison of the microstructure and properties of the FCAW and FCB welding technologies have rarely been investigated. It is thus significant to study the influence of the large difference between the welding heat inputs of the above two welding technologies on the microstructure and properties of TMCP EH36 high strength steel welding joints, to seek practical welding technology for TMCP EH36 steel.

2. EXPERIMENTAL

TMCP EH36 steel was the base material with a size of 300 mm×150 mm×32 mm, assembled with a V groove of 39° for FCAW and 50° for FCB, respectively, as seen in Fig. 1. The chemical composition of the steel by weight percentages was 0.07 C, 1.47 Mn, 0.15 Si, 0.13 Ni, 0.07 Cr, 0.005 P, 0.002 S, with trace amounts of Nb, Cu, Ti, and N, and a remaining balance of Fe. The carbon equivalent (CE) was calculated as 0.35 according to the equation: CE = C + Mn/6 + Cr + Mo + V/5 + Cu + Ni/15. EH36 steel with a yield strength of 515MPa is usually used for the construction of ship structures, and the details are shown in Tab. 1.

For the FCAW technology, CHT711 flux-cored wire with a diameter of 1.2mm was chosen, and pure CO_2 gas with a flow of 15L/min was used for protection. The details of the welding parameters are shown in Tab. 2. For the FCB technology, Y-DL flux-cored wire produced by NIPPON STEEL was used. The lead wire and the middle wire each had the same diameter of 4.8 mm, and the back wire had a diameter of 6.4 mm. The surface and pad flux were NSH-55ER and NSH-1RM,

respectively. The welding parameters were as follows: the voltage and the current of the front wire were 1340 V and 35 A, respectively; the voltage and the current of the middle wire were 1170 V and 41 A, respectively; the voltage and the current of the back wire were 1280 V and 47 A, respectively; the welding speed was 50cm/min. The weld joints were cooled in the air at room temperature after welding.

The microhardness of the joints were tested using a DHV-1000Z micro Vickers hardness tester according to the lines marked a and b in Fig. 2, with a 200 g load and 20 s of loading time. Starting from 15 mm on the left side of the welding joint, a Vickers hardness value was acquired every 1mm at each line-a and line-b site for 60 points along the horizontal direction of the joints. Electrochemical impedance spectroscopy (EIS) test samples were prepared from the center of the welded metal (WM) along the longitudinal direction via linear cutting into a size of 90 mm×10 mm×0.5 mm, marked as line 1 in Fig. 2. Before the EIS tests, the samples were polished using 2000 grid sandpaper, degreased with acetone, washed with distilled water, and dried with a blower. The working areas of the tested samples were prepared as 1cm^2, and the other parts of the samples were sealed with wax. The EIS testes were carried out using an Autolab PGSTAT302N electrochemical workstation with a three-electrode system. The working electrode was the tested sample (1 cm^2 working area), the auxiliary electrode was a Pt plate, the reference electrode was Ag/AgCl (3 mol/L KCl). The electrolyte was a 3.5 wt.% NaCl aqueous solution. Before testing, the working electrode was soaked in the electrolyte at the open circuit potential (OCP) mode for 30 min. The EIS mode was set at the OCP with a frequency of 10^{-2}~10^4 Hz, and an AC drive signal amplitude of ±5 mV. Each sample was observed and analyzed using an optical microscope (OM), a JXA-8100 scanning probe microscope (SEM) and S3700 SEM.

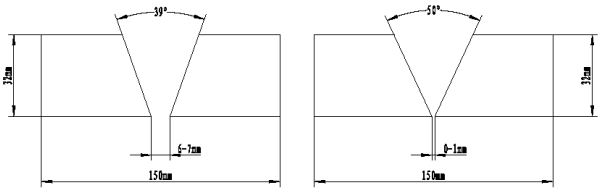

Figure 1. Sketched maps of the groove used in the (a) FCAW and (b) FCB technologies.

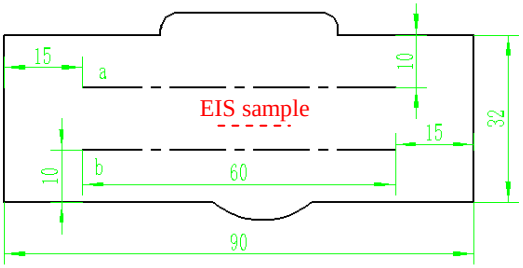

Figure 2. Conditions of the sampling positions for the microhardness tests and EIS tests.

Table 1. Mechanical properties of TMCP EH36 steel.

Yield Strength(MPa)	Tensile Strength(MPa)	Elongation rate(%)	-40°C Impact Energy(J)

15	580	22	190~280

Table 2. Welding parameters of the FCAW technology.

Layer	Pass	Current (A)	Voltage (V)	Speed (cm/min)	Interpass temperature (°C)	Gas flow (L/min)
1	1	160	26	6.7	150	15
2	2	220	28	20	190	15
3	3	220	28	16.7	156	15
4	4	230	28	16.4	150	15
5	5	240	28	13.3	160	15
6	6	210	27	18.8	170	15
	7	205	27	18.8	170	15
7	8	220	27	15.7	170	15
	9	215	27	11.3	170	15
8	10	200	27	14.5	180	15
	11	210	27	11.2	-	15

3. RESULTS AND DISCUSSION

3.1. Microstructure analysis

The microstructure of the metals welded using the FCAW and FCB technologies and the TMCP EH36 base metal were observed using OM and SEM, and the results are shown in Fig. 3. The microsturcture of the FCAW welded metal (Fig. 3a and Fig. 3c) consisted of acicular ferrite surrounded with primary austenite boudaries. There is a clear granular ferrite layer with a large grain size and ferrite slide plates that resulted from the welding heat inputs of the following welding passes of the multi-layer and multi-pass FCAW welding. With the low welding heat input (calculated as 18kJ/cm) of the FCAW technology, the cooling speed and supercooling rate were low enough to promote the growth of acicular ferrite (AF) to form the large granular ferrite (GF) and the ferrite slide plates (FSP). Fig. 3b and Fig. 3e show the microstructures of the FCB welded metal, and this was mainly acicular ferrite with primary austenite boundaries. It was observed that the grain size of the FCB welded metal was uniform with a relatively small average size of 30μm. The transformation of austenite to ferrite was thorough and rapid, and this was similar to the results reported by Yan et al. [10]. The welding heat input of the FCB technology in this study was extremely high (190kJ/cm), and this resulted in a high cooling rate and a high supercooling ratio. This contributed to the shrinking of the primary ausinite and the secondary phase particles, such as the martensite-austenite constituent (M-A) or the nonmetallic inclusions, seen as dark spots in Fig. 3.

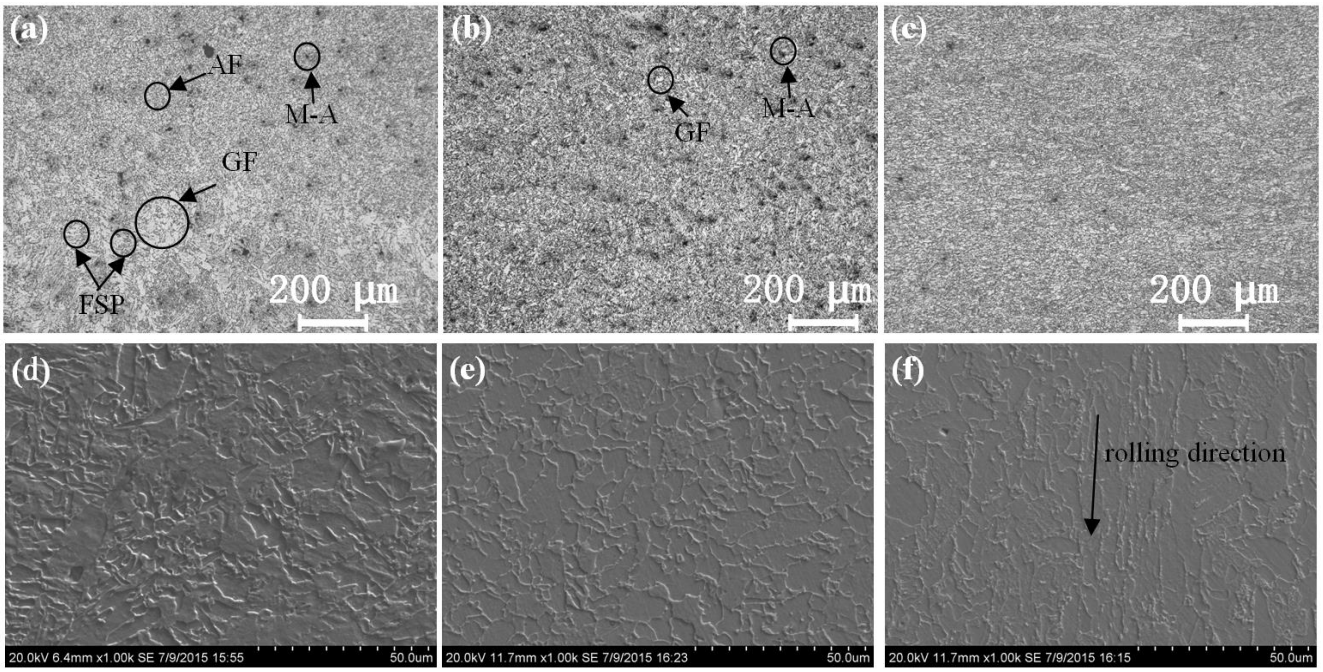

Figure 3. OM images of the microstructures of (a) the FCAW welded metal, (b) the FCB welded metal, and (c) the EH36 base metal. SEM images of the microstructures of (d) the FCAW welded metal, (e) the FCB welded metal, and (f) EH36 base metal.

The M-A islands or the inclusions in the FCB welded metal had a more uniform distribution than those in the FCAW welded metal, and this further reduced the nucleations and the free energy of the interface. The combination of these factorswas favorable for nucleation and the formation of the acicular ferrite and inhibited the growth of the GF structure. In Fig. 3c and Fig. 3f, the microstructures of the TMCP EH36 steel consisted of acicular ferrite and polygonal ferrite with consistent length and direction and had several uniformly distributed M-A islands that were consistently in the rolling direction. These observations indicated that there is an advantage in using the TMCP technology during the manufacture of low-carbon low-alloy steel to fulfill the requirements of FCB high-heat input welding.

3.2. Microhardness distribution

The properties of the welding joint corresponded well with the microstructure, as each microstructure possessed a different hardness. The difference between the microhardness distributions in different zones of the FCAW and FCB welding joints were studied by testing the upper 10mm line-a and the lower 10mm line-b across the joints for 60mm. The results are mapped in Fig. 4. The softening point happened in the different areas of the welding joints, ie. In the case of FCAW, it is in welding zone, and for FCB, it is in heat-affected zone (HAZ). Furthermore, from Fig. 4a, it is clear that there was a difference in the microhardness between the upper and lower welded metal zone of the FCAW joint, and this was unavoidably caused by the multiple heat input characteristics of the multi-layer and multi-pass FCAW welding. The upper welded metal was influenced less by the extra welding heat input, which resulted in less softening with the microhardness value ranging from 165~195Hv,

compared with the lower welded metal, where the microhardness value ranged from 173~204Hv. In the FCAW welded metal zone, the softening phenomenon was even more severe in the lower welded metal. The maximum microhardness difference was as high as 39Hv in the FCAW welded metal. For the different welded metal zones in the FCB joint, it was found (Fig. 4b) that the microhardness in both the upper and lower welded metal zones ranged from 192~223Hv with a slight fluctuation in the symmetric distribution. The microhardness distributions in the FCB welding joint were similar in the upper line a and the lower line b, within a relatively narrow and slight variation range of the microhardness. There was an obvious microhardness trough around the fusion zone ranging from 160~205Hv, and this became a wave crest with a peak of 225Hv around 18mm from the fusion line. The trough value of 160Hv was around 10mm from the fusion line. The softening phenomenon happened in the HAZ of the FCB welding joint and resulted from the high welding heat input of FCB technology. In the case of FCB welding, it is necessary to consider the effect of the high welding heat input on the EH36 base metal.

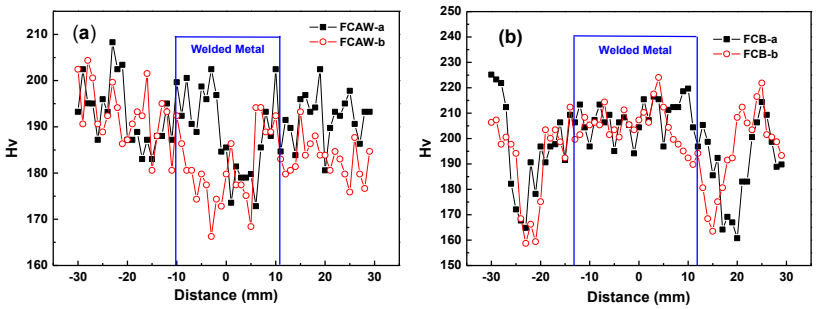

Figure 4. Microhardness distributions along the crosssections of the (a) FCAW and (b) FCB welding joints.

3.3. Electrochemical behavior

The EIS responses of the FCAW and FCB welded metals and the EH36 base metal in a 3.5% NaCl solution at open circuit potentials were done to study the differences in the electrochemical behavior. The results are shown as Nyquist, Bode, and Bode-phase plots in Fig. 5. To reduce the interference of external factors, the OCP tests were carried out for 30min with each sample before the EIS tests. It was found that the potential response of each sample gradually decreased until reaching a relatively constant state after 300s during the OCP test.

The Nyquist plots of all of the samples have imperfect semicircles (Fig. 5a), which represent the capacitive arcs. The diameter of the imperfect semicircle corresponding to the EH36 base metal was largest, and this means the base metal had the largest capacitive arc and indicates that it had the best passivation behavior. The diameter of the imperfect semicircle corresponding to the FCB welded metal was higher than that of the FCAW welded metal. This clearly shows that the larger capacitive arcs were produced by the increase in the welding heat input, and this means that the FCB welded metal had a stronger corrosion resistance than the FCAW welded metal. At the low frequency range of

the Bode plots (Fig. 5b), the sample with a higher electrical resistance value had a stronger corrosion resistance, and these results are consistent with the analysis from the above Nyquist plots.

As seen in Fig. 5c, the Bode-phase curves of both of the welded metals and the base metal show certain constant values in the middle frequency range. Also, the maximum phase angle values remained close to 55°, which indicates the formation and growth of the oxide films in the middle frequency range, according to Melchers [11], who confirmed similar capacitive responses of the welded metals and the base metal. All phase angle values remained far below 80°, which also indicates that the capacitive response was not pure or ideal, and this was similar to the results reported by Fernández-Domene et al. [12]. The formation of an oxide film plays a major role in the corrosion mechanism. There were phase lags with a frequency in the middle to high frequency range in the order of: the EH36 base metal, the FCB welded metal, and the FCAW welded metal. This corresponds to the relative order of ability to form an oxide film.

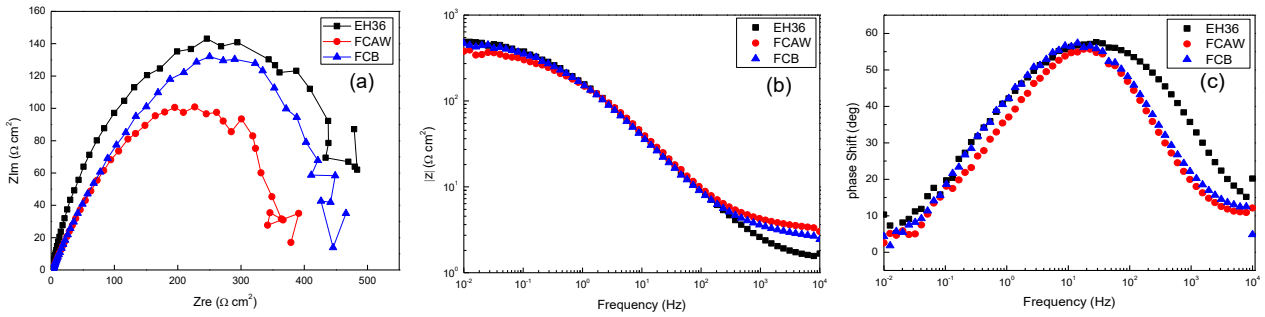

Figure 5. (a) Nyquist, (b) Bode, and (c) Bode-phase plots of the FCAW and FCB welded metals and the EH36 base metal in a 3.5 wt.% NaCl solution at the open circuit potentials.

To simulate the measured impedance data, an equivalent circuit was used and is shown in Fig. 6. The variations in the impedance parameters are shown in Tab. 3. In this equivalent model, R_s is the solution resistance and represents the ability to form an oxide film. R_{ct} represents the charge transfer resistance of the metal for the electrolyte, which is defined as the corrosion resistance of the sample in the electrolyte. C_{PE} represents the constant phase element corresponding to the metal, as supported by Soltis and Lichti [13].

The variation in the impedance parameters of the EH36 base metal and the FCB and FCAW welded metals in a 3.5% NaCl solution is illustrated in Table 3. There was a rule of inverse proportions for the R_s values and R_{ct} values. The EH36 base metal had the highest R_{ct} value of 492.8 $\Omega \cdot cm^2$ and the lowest R_s value of 1.3 $\Omega \cdot cm^2$, meaning that the EH36 base metal possessed a greater tendency to form an oxide film than the welded metals did. Once a dense oxide film formed and grew into a stable state, it inhibited the charge transfer process from the metal to the electrolyte. This appeared as a higher R_{ct} value and reflected a higher corrosive resistance. Apparently, the uniform organizational structure of the EH36 base metal helped form a dense oxide film. It was concluded that Rs represents the ability to form an oxide film and that R_{ct} represents the anti-corrosion capability. The FCB WM with a relatively uniform microstructure benefited from the welding with one-pass high welding heat input and had a stronger corrosive resistance than the FCAW WM, which is clear from its higher R_{ct} value of 442.6

$\Omega \cdot cm^2$ compared to that of the FCAW counterpart, which was 364.0 $\Omega \cdot cm^2$. Both of the two WMs had lower corrosive resistance, due to the oxide film deterioration effect caused by particles such as the M-A islands or the inclusions in the welded metals. Furthermore, the large FSP microstructure had difficulty forming an oxide film rapidly, and this resulted in the lowest R_{ct} of the FCAW WM.

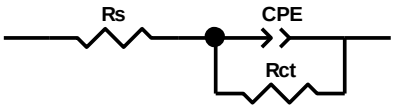

Figure 6. Best equivalent circuit used to model the experimental EIS data for the FCAW and FCB welded metals and the EH36 base metal.

Table 3. Variations in the impedance parameters of the EIS tested samples.

	R_s ($\Omega \cdot cm^2$)	C_{PE}-T (mf)	C_{PE}-P	R_{ct} ($\Omega \cdot cm^2$)
EH36 BM	1.3	1392.1	0.688	492.8
FCB WM	2.6	1393.1	0.706	442.6
FCAW WM	3.1	1311.4	0.701	364.0

To understand the above observations, the corrosive morphologies of the WMs were observed after the EIS tests, and the results are shown in Fig. 7. There were no corrosion products observed on the FCAW WM surface, and obvious residual corrosion products still covered the FCB WM surface. These observations are consistent with the above EIS results. According to the phase-corrosion mechanism of Ha et al. [14] and Qu et al. [15], the corrosion originated at the grain boundaries between the austenite and ferrite structures or at the interface between the inclusions and the matrix followed by the ferrite etching in the primary austenite boundaries or in the matrix around the inclusion. Thus, formation of an oxide film at those sites tended to be inhibited. Formation of the oxide films on the FCAW WM was inhibited and exposed the fresh metal directly in the electrolyte. The continued growth of oxide films accumulated and covered the FCB WM surface to prevent further corrosion and finally evolved into the residual corrosion products, and this effectively improved the anti-corrosive ability.

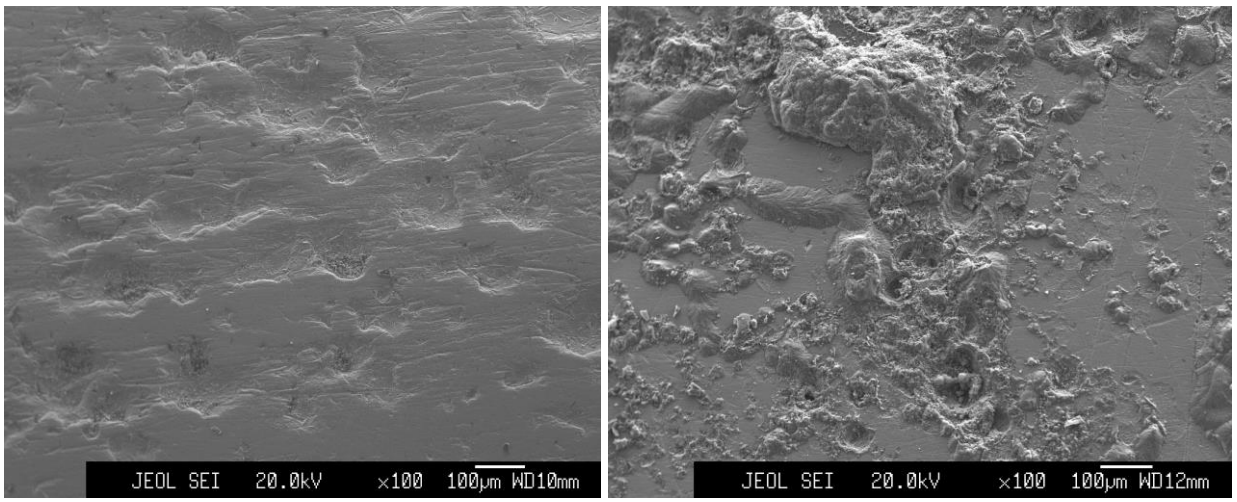

Figure 7. Corrosion morphologies of (a) the FCAW welded metal and (b) the FCB welded metal after EIS tests.

4. CONCLUSIONS

The purpose of this work was to investigate the influence of the welding heat input of FCAW and FCB welded metals and EH36 high strength steel. Acicular ferrite was distributed with abundant secondary phase particles dominating the welded metal of the FCB joints and contributing to the characteristics of the high welding heat input one-pass welding formation. The result was stronger electrochemical impedance behavior in a 3.5% NaCl solution compared to that of the FCAW counterpart. The softening phenomenon occurred at the heat-affected zone of the FCB joints and the welded metal zone of the FCAW joints. Irrespective of the welding technology, the EH36 base metal had stronger corrosion resistance than the welded metal because of the uniform microstructure. Such organizations as GF, inclusions, M-A islands, and especially the FSP phase in the WMs inhibited the formation of an oxide film and deteriorated the corrosive resistance.

ACKNOWLEDGMENTS

This research was supported by the National Natural Science Foundation of China (no. 51601043), the Scientific Program of GDAS (2016GDASPT-0205), the technical project of Guangdong and Guangzhou (2014B050503004, 2016B090918120, 201704030112, 201604046026)

References

1. S.H. Wang, C.C. Chiang and S.L.I. Chan, *Mater. Sci. Eng. A.*, 344 (2003) 288.
2. H. Xie, L.X. Du, J. Hu and R.D.K. Misra, *Mater. Sci. Eng. A.*, 612 (2014) 123.
3. C.H. Lee, H.S. Shin and K.T. Park, *J. Constr. Steel Res.*, 74 (2012) 134.
4. C. Roepke, S. Liu, S. Kelly and R. Martukanitz, *Welding Journal*, 89 (2010) 140S.
5. L.W. Tsay, T.S. Chern, C.Y. Gau and J.R. Yang, *Inter. J. Fatigue.*, 21 (1999) 857.
6. L.R. Bhagavathi, G.P. Chaudhari and S.K. Nath, *Mater. Des.*, 32 (2011) 433.
7. J. Hu, L.X Du, J.J. Wang and C.R. Gao, *Mater. Sci. Eng. A*, 577 (2013) 161.
8. Y. Zhang, C. Jia, B. Zhao, J. Hu and C.S. Wu, *J. Mater. Process. Technol.*, 238 (2016) 373.
9. X.Z. Chen, Y.Y. Fang, P. Li, Z.Z. Yu, X.D. Wu and D.S. Li, *Mater. Des.*, 65 (2015) 1214.
10. N. Yan, S.F. Yu and Y. Chen, *Sci. Technol. Weld. Joining*, 20 (2015) 418.
11. R.E. Melchers, *Corros. Sci.*, 48 (2006) 4174.

12. R.M. Fernández-Domene, E. Blasco-Tamarit, D.M. García-García and J. García-Antón, *Thin Solid Films*, 558 (2014) 252.
13. J. Soltis and K.A. Lichti, *Corros. Sci.*, 68 (2013) 162.
14. H.Y. Ha, M.H. Jang, T.H. Lee and J. Moon, *Corros. Sci.*, 89 (2014) 154.
15. S.P. Qu, X.L. Pang, Y.B. Wang and K.W. Gao, *Corros. Sci.*, 75 (2013) 67.